Soft Matter

Cell Motility Dependence on Adhesive Wetting

Journal:	*Soft Matter*
Manuscript ID	SM-ART-09-2018-001832.R2
Article Type:	Paper
Date Submitted by the Author:	25-Jan-2019

Complete List of Authors:	Cao, Yuansheng; University of California San Diego, Department of Physics Karmakar, Richa; University of California San Diego Ghabache, Elisabeth; University of California San Diego Gutierrez, Edgar; UCSD, Physics Zhao, Yanxiang; The George Washington University, Department of Mathematics Groisman, Alex; UCSD, Physics Department Levine, Herbert; Rice University, Bioengineering Camley, Brian; Johns Hopkins University Rappel, Wouter-Jan; UC San Diego, Physics

Soft Matter

ARTICLE TYPE

Cite this: DOI: 10.1039/xxxxxxxxxx

Cell Motility Dependence on Adhesive Wetting†

Yuansheng Cao,[a‡] Richa Karmakar,[a‡] Elisabeth Ghabache,[a] Edgar Gutierrez,[a] Yanxiang Zhao,[b] Alex Groisman,[a] Herbert Levine, [c] Brian A. Camley,[d] and Wouter-Jan Rappel[a*]

Received Date
Accepted Date

DOI: 10.1039/xxxxxxxxxx

www.rsc.org/journalname

Adhesive cell-substrate interactions are crucial for cell motility and are responsible for the necessary traction that propels cells. These interactions can also change the shape of the cell, analogous to liquid droplet wetting on adhesive substrates. To address how these shape changes affect cell migration and cell speed we model motility using deformable, 2D cross-sections of cells in which adhesion and frictional forces between cell and substrate can be varied separately. Our simulations show that increasing the adhesion results in increased spreading of cells and larger cell speeds. We propose an analytical model which shows that the cell speed is inversely proportional to an effective height of the cell and that increasing this height results in increased internal shear stress. The numerical and analytical results are confirmed in experiments on motile eukaryotic cells.

1 Introduction

Migration of eukaryotic cells plays an important role in many biological processes including development[1], chemotaxis[2], and cancer invasion[3]. Cell migration is a complex process, involving external cues, intra-cellular biochemical pathways, and force generation. The adhesive interaction between cells and their extracellular environment is an essential part of cell motility[4] and is generally thought to be responsible for frictional forces necessary for propulsion[5,6]. These frictional forces are due to the motion of the cytoskeleton network and can be measured by traction force microscopy[7]. On the other hand, adhesive cell-substrate interaction can also lead to cell spreading in both moving and non-moving cells[8–10]. This is similar to the spreading of a liquid droplet during the wetting of an adhesive substrate. The resulting changes of the cell shape can potentially affect cell motility. Experimentally, it is not possible to decouple the effect of adhesion and friction, making it challenging to quantify the relative importance of spreading in cell motility.

Here we investigate the dependence of motility on cell-substrate adhesion using a mathematical model in which we can alter the adhesive forces independent of frictional forces. We carry out numerical simulations of this model using the phase field approach, ideally suited for objects with deforming free boundaries[11,12]. We focus on a 2D vertical cross-section of a migrating cell which captures both cell-substrate interactions and internal fluid dynamics[13]. Our adhesive interactions are based on the phase-field description of wetting[14,15] and are independent of the molecular details of cell-substrate adhesion. Our simulations, together with an analytical 2D model extended from a previous 1D model[16], generate several nontrivial and testable predictions which are subsequently verified by experiments using motile *Dictyostelium discoideum* cells.

2 Results

2.1 Model

Our vertical cross-sectional model cell captures the interaction of the cell with the bottom and, possibly, top substrate, as well as the interior of the cell[13] (Fig. 1). This is in contrast to most computational studies of cell motility which model a flat cell that is entirely in contact with the substrate[17–20]. This interior consists of a viscous cytoskeleton and is described as a compressible actin fluid[21] with constant viscosity while cell movement is driven by active stress, located at the front of the cell. Note that we do not consider myosin-based contraction. Furthermore, and following Ref.[21], we neglect the coupling between the actin fluid (representing the cytoskeleton) and the cytoplasm. The latter is assumed to be incompressible, resulting in volume conservation. This type of model which treats the cytoskeleton as an active viscous compressible fluid has been used in several recent

[a] Department of Physics, University of California, San Diego, La Jolla, California 92093, USA.
[b] Department of Mathematics, The George Washington University, Washington, DC 20052, USA.
[c] Department of Bioengineering, Center for Theoretical Biological Physics, Rice University, Houston, Texas 77005, USA.
[d] Department of Physics & Astronomy and Department of Biophysics, Johns Hopkins University, Baltimore, Maryland 21218, USA.

† Electronic Supplementary Information (ESI) available: [details of any supplementary information available should be included here]. See DOI: 10.1039/cXsm00000x/

‡ These authors contributed equally to this work. ∗ Email: rappel@physics.ucsd.edu

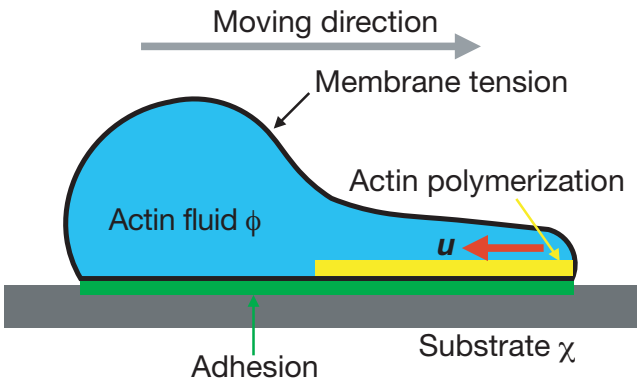

Fig. 1 Schematic illustration of a model cell on a substrate. The cross-section of the cell is represented by a phase field ϕ while the substrate is defined by a field χ. The dynamics of the cytoskeleton network is modeled as an actin fluid with velocity $\mathbf{u}$ (red arrow). Forces in the model include the membrane tension, cell-substrate adhesive forces, forces due to active actin polymerization, and cytosolic viscous forces (proportional to $\mathbf{u}$). Actin polymerization is restricted to a narrow region near the substrate at the cell front-half, as indicated by the yellow band. Additional model details are given in main text and in Supplemental Material.

studies[22–26]. Friction is caused by the motion of the cytoskeleton relative to the substrate and is taken to be proportional to the actin fluid velocity. To accurately capture cell shape and its deformations, we use the phase field approach in which an auxiliary field $\phi(\boldsymbol{r},t)$ is introduced to distinguish between the interior ($\phi = 1$) and exterior ($\phi = 0$). This approach allows us to efficiently track the cell boundary which is determined by $\phi(\boldsymbol{r},t) = 1/2$[12,20,24,25,27,28]. In our model, boundary motion is driven by fluid flow which is determined by adhesion, friction, membrane forces and active protrusion. The cell is placed on a substrate which is parallel to the x direction, and polarized in one direction. As described in earlier work[24,25,29], the evolution of the cell's shape is determined by the phase field dynamics:

$$\frac{\partial\phi(\boldsymbol{r},t)}{\partial t} = -\boldsymbol{u}\cdot\nabla\phi(\boldsymbol{r},t) + \Gamma(\varepsilon\nabla^2\phi - G'/\varepsilon + c\varepsilon|\nabla\phi|), \qquad (1)$$

where the advection term couples the velocity field of the actin fluid, $\boldsymbol{u}$, to the phase field, ε is the width of the boundary, Γ is a relaxation coefficient, G is a double-well potential with minima at $\phi = 1$ and $\phi = 0$, and c is the local curvature of the boundary (see Supplemental Material).

The actin fluid velocity field is determined by the stationary Stokes equation with an assumption of perfect compressibility (zero pressure)[21]:

$$\nabla\cdot[\nu\phi(\nabla\boldsymbol{u} + \nabla\boldsymbol{u}^T)] + \boldsymbol{F}_{sub} + \boldsymbol{F}_{mem} + \boldsymbol{F}_{area} + \nabla\cdot\sigma^a = 0, \qquad (2)$$

where ν is the viscosity of the cell and where σ^a is the active stress due to actin polymerization, further detailed below. Here, we have also neglected inertial forces, an approximation that is valid on the cellular scale where the Reynolds number is very small compared to 1[21,23]. Furthermore, the validity of this approximation has been explicitly verified in previous studies[21,24]. $\boldsymbol{F}_{sub}$ is the interaction between the cell and substrate and contains both adhesion and friction, $\boldsymbol{F}_{sub} = \boldsymbol{F}_{adh} + \boldsymbol{F}_{fric}$. The adhesive force is given by $\boldsymbol{F}_{adh} = \frac{\delta H(\phi,\chi)}{\delta\phi}\nabla\phi$, with the cell-substrate interaction potential:

$$H(\phi,\chi) = \int d\boldsymbol{r}^2\phi^2(\phi-2)^2W(\chi).$$

Here, $\chi(\boldsymbol{r})$ is a constant field which marks the substrate (or ceiling) and continuously changes from $\chi = 1$ (within the substrate) to $\chi = 0$ (out of substrate; Fig. S1). $W(\chi)$ is a potential with a negative adhesion energy per unit length controlled by a parameter A such that larger values of A represent a larger adhesive force between cell and substrate. In addition, this potential contains a short-range repulsion that ensures that the cell does not penetrate the substrate. The term $\phi^2(\phi-2)^2$ is added to ensure that the force peaks within the boundary and vanishes at $\phi = 0$ and $\phi = 1$.

The second term in $\boldsymbol{F}_{sub}$ describes the frictional force between the cell and the substrate. Depending on the cell type, these forces can arise from focal adhesions or from non-specific cell-substrate interactions. For simplicity, the frictional force in our cross-sectional model is modeled as a viscous drag proportional to the actin fluid velocity :

$$\boldsymbol{F}_{fric} = -\xi_s\chi\boldsymbol{u} - \xi_d\boldsymbol{u},$$

where the first term is the cell-substrate friction, parameterized by the coefficient ξ_s, and the second term represents a damping force, introduced to increase numerical stability. We have verified that the cell speed changes little when we vary the drag coefficient ξ_d (Fig. S2). Initially, we will vary both the adhesion energy (which controls spreading) and the frictional drag separately, allowing us to determine its relative contribution to cell motility. We will then examine model extensions which implement dependent adhesion and friction mechanisms (see Fig. 4). The uniform membrane tension $\boldsymbol{F}_{mem}$ and a force arising from cell area conservation $\boldsymbol{F}_{area}$ are introduced as in our previous work[25,27]. The latter force results in cell shapes with roughly constant area. More details of these forces, along with details of the simulation techniques for Eqns. (1&2) are given in Supplemental Material. As a consistency check, we have simulated cells without any propulsive force and have verified that the resulting static shapes agree well with shapes obtained using standard energy minimization simulations[30] (Fig. S3).

Polarization in our model is introduced through the polarization indicator ρ_a. In contrast to our previous studies[24,25], we do not explicitly include diffusion or advection of this indicator and, for simplicity, have chosen $\rho_a = 1$ at the front half and $\rho_a = 0$ at the rear half of the cell. Following earlier work[13,31,32], we assume that protrusions that are generated by actin polymerization only occur at the front of the cell and close to the substrate. Our formulation of the active stress σ^a incorporates these assumptions. Specifically, we introduce a field $\psi(\boldsymbol{r})$ with width λ and located a distance ε away from the substrate (Fig. S1). By making the active stress proportional to $G(\psi)\phi\rho_a(\boldsymbol{r})$, we restrict possible protrusions to a narrow band parallel to the substrate and in the cell front. This band is schematically shown in yellow in Fig. 1. In addition, we localize the stress to the interface by multiplying the

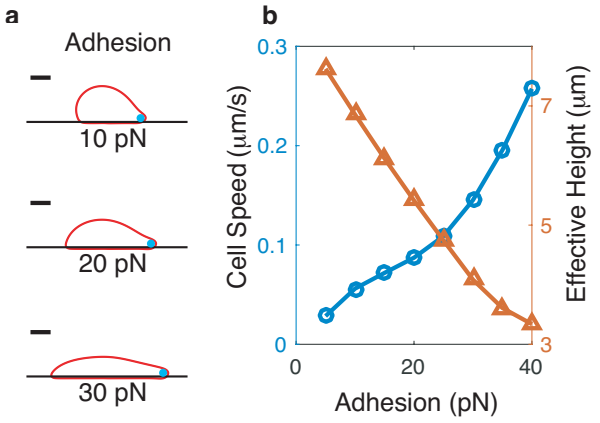

Fig. 2 a, Cell shapes for different values of substrate adhesion strength. The blue dots here, and elsewhere, schematically indicate the location of active stress. Scale bar $5\mu m$. **b**, Cell speed (blue circles) and effective height of a cell (red triangles) as a function of the adhesion strength.

expression of σ^a by the factor $|\nabla\phi|^2$. This is schematically shown as blue dots in Figs. 2 and 3. The expression for the stress is then given by:

$$\sigma^a = -\eta_a G(\psi)\phi\rho_a(\boldsymbol{r})\varepsilon|\nabla\phi|^2\hat{\boldsymbol{n}}\hat{\boldsymbol{n}}. \tag{3}$$

Here, η_a is the protrusion coefficient, and $\hat{\boldsymbol{n}} = \nabla\phi/|\nabla\phi|$ is the normal to the cell boundary. Note that our model does not include any possible feedback between substrate and stress generation.

Our simulations are carried out as described previously[25] and further detailed in the Supplemental Material where we also list the full set of equations. As initial conditions, our simulations start with polarized cells in which the distribution of ρ_a is asymmetric. The cell's speed is tracked by $\boldsymbol{v}_c = d\boldsymbol{x}_c/dt$ with $\boldsymbol{x}_c$ the cell mass center $\boldsymbol{x}_c = \int \boldsymbol{x}\phi d^2\boldsymbol{r}/\int\phi d^2\boldsymbol{r}$ and simulations are continued until a steady state has been achieved. Parameters values used in the simulations are given in Table S1.

2.2 Simulation results and analysis

We first investigate how cells move on a single substrate with different adhesion energies. For this, we solve the phase field equations for different values of the adhesion parameter A. Examples of resulting cell shapes are shown in Fig. 2 while an example of the actin fluid velocity field is shown in Fig. S4. We find that with increasing adhesion strength, cells spread more and thus become thinner, similar to the spreading of a droplet on surfaces with increasing wettability (Fig. 2a). Our simulations reveal that the cell speed (i.e., the velocity parallel to the substrate) keeps increasing as the adhesion increases, without any indication of saturation (Fig. 2b). This is perhaps surprising, as our physical intuition suggests that adhesion and friction go hand in hand, with larger adhesion corresponding to higher friction. In our simulations, however, adhesion and friction are independent and can be separately adjusted.

To provide insights into the relation between adhesion, cell shape and speed, we consider a simplified version of Eq. (2), similar to the 1D model examined in Ref.[16]. Since only asymmetric stress will contribute to the cell's speed[33], we only need to take into account the viscosity, friction and active stress in the equation:

$$\nu\nabla\cdot\sigma^{vis} - \xi\boldsymbol{u} + \nabla\cdot\sigma^a = 0, \tag{4}$$

where $\sigma^{vis} = \nabla\boldsymbol{u} + \nabla\boldsymbol{u}^T$, ξ is a friction coefficient taken to be spatially homogeneous, and σ^a is the active stress which is 0 outside the cell. Boundary conditions include a steady cell shape $\hat{\boldsymbol{n}}\cdot\boldsymbol{v}_c = \hat{\boldsymbol{n}}\cdot\boldsymbol{u}$, zero net traction force $\int\xi\boldsymbol{u}d^2\boldsymbol{r} = 0$, and zero parallel stress $\sigma^{vis}\cdot\hat{\boldsymbol{t}} = 0$, where $\hat{\boldsymbol{n}},\hat{\boldsymbol{t}}$ are the normal and tangential unit vector, respectively.

It is in general not possible to solve Eq. 4 in a arbitrary geometry. However, for the special case of a fixed-shape rectangular cell with length L and height H occupying $x\in[-L/2,L/2], y\in[0,H]$ we can solve for the cell speed v_c (see the Supplemental Material). By averaging the stress over the vertical direction and following Carlsson's one-dimensional solution[16], we find:

$$v_c = -\frac{1}{4\nu H}\int_{-L/2}^{L/2}\frac{\tilde{\sigma}^a_{xx}\sinh(\kappa x)}{\sinh(\kappa L/2)}dx, \tag{5}$$

where $\kappa = \sqrt{\xi/(2\nu)}$ determines the spatial scale of the decay of a point stress source[16] and where $\tilde{\sigma}^a_{xx} = \int_0^H\sigma^a_{xx}dy$ (see also the Supplemental Material). From this solution it is clear that asymmetric active stress distribution will lead to cell motion. When $\kappa L/2 \ll 1$, corresponding to a highly viscous cytoskeleton[34], the speed is proportional to the normalized active stress dipole $1/(LH)\times\int x\tilde{\sigma}_{xx}dx$. In the phase field model, the active stress in Eq. 3 is a negative bell shape function located at the front tip of the cell. This active stress can be approximated by $\tilde{\sigma}_{xx} = -\lambda\beta\delta[x-(L/2)_-]$ where β is the active stress strength and where the stress is assumed to be located just inside the cell (see the Supplemental Material and Ref.[16]). Substituting this into Eq. 5, we find

$$v_c = \frac{\lambda\beta}{4\nu H}, \tag{6}$$

which shows that the cell speed scales inversely with the height of the cell, and that this scaling is independent of the cell length. Of course, a real cell will not be rectangular, and in the Supplemental Material we show that the cell speed scales with the average height for a more complex-shaped cell (Fig. S5). This suggests that the cell speed can be parameterized using an effective height H_{eff}, which can be computed by averaging the height over the cell length: $H_{\text{eff}} = (1/L)\int H(x)dx$. In Fig. 2b we see that H_{eff} is monotonically decreasing when adhesion increases. The inverse relation between cell speed and effective height qualitatively agrees with the above analysis.

Interestingly, the above found relation between cell speed and cell height does not depend on the way the cell's effective height is altered. To verify this, we also simulated cells in confined geometries in which they are "squeezed" between two substrates, as shown in Fig. 3a (an example of a cell with the actin fluid velocity field can be found in Fig. S4). Consistent with our analytical results, we find that as the chamber height is reduced, the cell's speed increases while the cell's effective height decreases (Fig. 3b). Furthermore, changing the adhesive strength on the top and bottom substrate while keeping the distance between them fixed

will also affect the cell shape and its effective height (Fig. 3c and Fig. S4). Our simulations show that a difference in the top and bottom adhesion leads to an asymmetric cross-section and that the cell's effective height reaches a maximum for equal top and bottom adhesion (Fig. 3d). Consistent with Eq. 6, our simulations show that the cell speed reach a minimum for substrates with equal adhesive strengths (Fig. 3d).

Our results can be explained by realizing that cells contain a cytoskeleton network that can be described as a compressible viscous actin fluid. This actin fluid contains "active" regions which are confined to a layer with fixed width of λ, and "passive" regions that are outside these active regions. Active stress is only generated within this active region. Large viscosity will make the cell speed independent of cell length (see Eq. 5 and Ref. [16]). However, this viscosity also leads to dissipation due to internal shear stress: passive regions are coupled to the active regions through vertical shear interactions, resulting in dissipation. This dissipation increases with increasing cell height, as can also be seen in the velocity profile shown in Fig. S6, and thinner cells will move faster. We have tested this explanation by carrying out additional simulations. In one set, we simulated cells moving in chambers of varying height while keeping the ratio of the size of the active stress layer λ and cell height constant. Consistent with our theoretical predictions, the speed of these cells is independent of the chamber height (Fig. S7). In addition, we have simulated cells in which the active stress region spans the entire front. Again in line with our theoretical insights, the cell speed was found to be largely independent of the chamber height (Fig. S8).

In our simulations, we have kept the friction coefficient constant and have thus ignored any potential link between adhesion and friction. This is likely appropriate for *Dictyostelium* cells but may not be valid for mammalian cells that have integrin mediated focal adhesions. The exact dependence of friction on adhesion is complicated and poorly understood[35,36]. Our model, however, can easily be extended to explore the entire phase space of friction and adhesion. To illustrate this, we compute the speed of a cell crawling on a single substrate by sampling a broad range of adhesion strengths ($A = 10$ pN to $A = 40$ pN) and friction coefficients ($\xi_s = 1$ Pa s/μm to $\xi_s = 10^3$ Pa s/μm) while keeping all other parameters fixed. The resulting cell speeds are shown in Fig.4a using a color map. As expected, cells stall when adhesion is low and friction is high (dark blue region) while the highest cell speed occurs for large adhesion and a relatively broad range of low friction values (yellow region).

Different dependencies between friction and adhesion correspond to different trajectories through the two-dimensional phase space of Fig. 4a. The results we have presented so far correspond to traversing the phase space along the white dashed line in Fig. 4a. The black dashed line in this figure, on the other hand, represents a linear dependence between friction and adhesion ($\xi_s = \xi_b + \xi_l A/A_l$ with ξ_b =1 Pa s/μm, ξ_l =5 Pa s/μm, and A_l =1 pN) while the red dashed line represents an exponential dependence ($\xi_s = \xi_b + \xi_e \exp(A/A_e)$ with ξ_b =1 Pa s/μm, ξ_e =1 Pa s/μm, and A_e =7 pN). For these two adhesion-friction dependencies, we have computed the cell speed for unconfined (Fig.4b) and confined cells (Fig.4c). For friction that depends linearly on adhesion, the speed of unconfined cells continues to increase as adhesion increases (black line in Fig.4b). This is very similar to the results we obtained for constant friction (cf. Fig. 2b). For exponential friction, the speed of unconfined cells initially increases for increasing adhesion. As adhesion increases, however, friction becomes more and more dominant, and cell's speed reaches a maximum, followed by a decrease (red line in Fig.4b). This bi-phasic dependence of adhesion is consistent with a variety of experiments[22,37–39]. For confined cells and a linear friction-adhesion relationship, the dependence of the cell speed on the adhesive strength of the bottom substrate is shown in Fig. 4.c (black line). Again, the results are very similar to our previously studied, constant friction case (cf. Fig.3d): cell speed reaches a minimum when the top and bottom adhesion strength are equal. Not surprisingly, the dependence of cell speed on bottom adhesion is different for the exponential relationship. Here, friction becomes dominant when adhesion increases, resulting in a cell speed that continuously decreases. These results show that friction plays a relatively small role in determining cell speed unless friction ξ_s increases over orders of magnitude when adhesion A changes by small amounts.

2.3 Experimental results

To test the above predictions, we performed motility experiments of *Dictyostelium discoideum* cells. Importantly, these cells, unlike mammalian cells, do not make integrin mediated focal adhesions and their substrate adhesion is likely to be mediated by direct physiochemical factors such as van der Waals attraction[40]. Experiments are carried out in microfluidic devices, as shown in Fig. 5a and modified from earlier work[41] (see also Supplemental Material and Fig. S9). Cells are moving in chambers with height h and with substrates that have variable adhesive properties. A constant cAMP gradient is established by diffusion so that cells preferably move in one direction (denoted as the x direction). Note that the constant signal polarizing the cell in one direction is consistent with our model of a constantly-polarized cell.

Dictyostelium cells move by extending actin filled protrusions called pseudopods which can extend over a significant distance from the substrate. As a consequence, our confined cells occlude the entire space between two substrates. This was verified explicitly by labeling the cell with a fluorescent membrane marker and creating confocal z-stacks (Fig. S10). The results also demonstrate that in the case of symmetric adhesion the outline of the cell does not change appreciably as one moves from one to the other substrate. Furthermore, using LimE as a fluorescent marker, we have verified that the level of actin polymerization is largest near the substrates (Fig. S10 C). This observation is in agreement with earlier experiments of *Dictyostelium* cells migrating in a narrow channel[32] which revealed significantly larger levels of LimE fluoresence near the channel walls.

The top substrate of the chamber consists of Polydimethylsiloxane (PDMS) and the bottom substrate is either made of PDMS or is coated with a thin layer of Polyethylene glycol (PEG) gel. Cells moving on these PEG-coated substrates have vastly reduced adhesion, as reported in earlier studies[42]. We measure the aver-

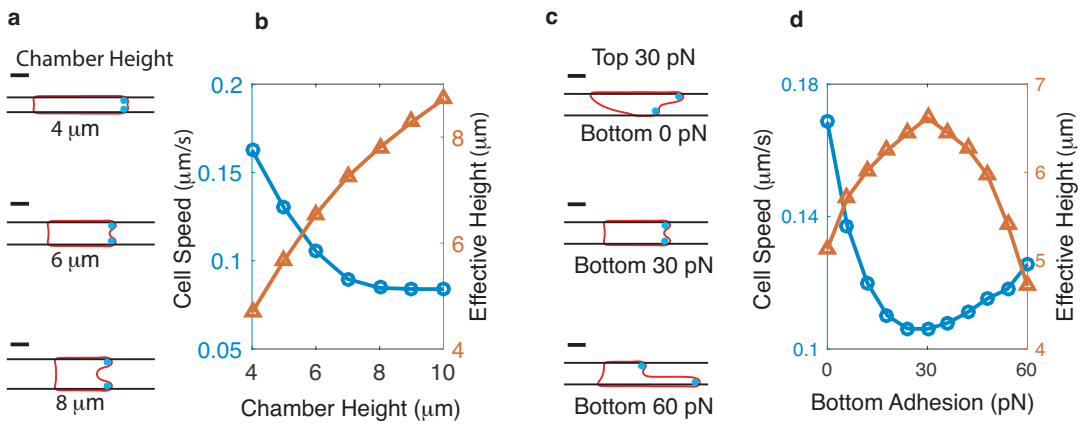

Fig. 3 a. Cell shapes for different chamber heights. The adhesion strength of the top and bottom substrate is fixed at 30 pN. Scale bar: $5\mu m$. **b**. Corresponding cell speed (blue circles) and effective height (red triangles) as a function of chamber height. **c**. Cell shapes in a chamber with adhesive top and bottom substrates, with the top substrate adhesion fixed to 30 pN. Scale bar: $5\mu m$. **d**. Cell speed (blue circles) and effective height (red triangles) as a function of adhesion strength of the bottom substrate (chamber height=6μm).

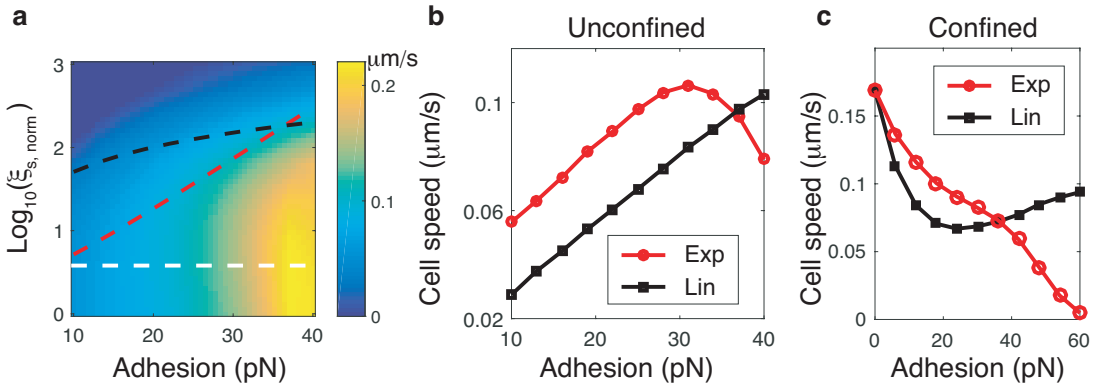

Fig. 4 a, Cell crawling speed dependence on adhesion strength and friction coefficient (normalized by ξ_s =1 Pa s/μm). Cell speed is visualized using the colormap. The dashed lines correspond to different dependencies of the friction on adhesion (white: constant friction, black: linear dependence, red: exponential dependence). **b**, Cell speed for unconfined cells as a function of adhesion for linear (black line) and exponential (red line) dependence on adhesion (for parameters see main text). **c**, Speed of confined cells as function of bottom substrate adhesion strength for linear (black line) and exponential (red line) dependence of friction on adhesion (top substrate adhesion=30 pN, chamber height=6μm).

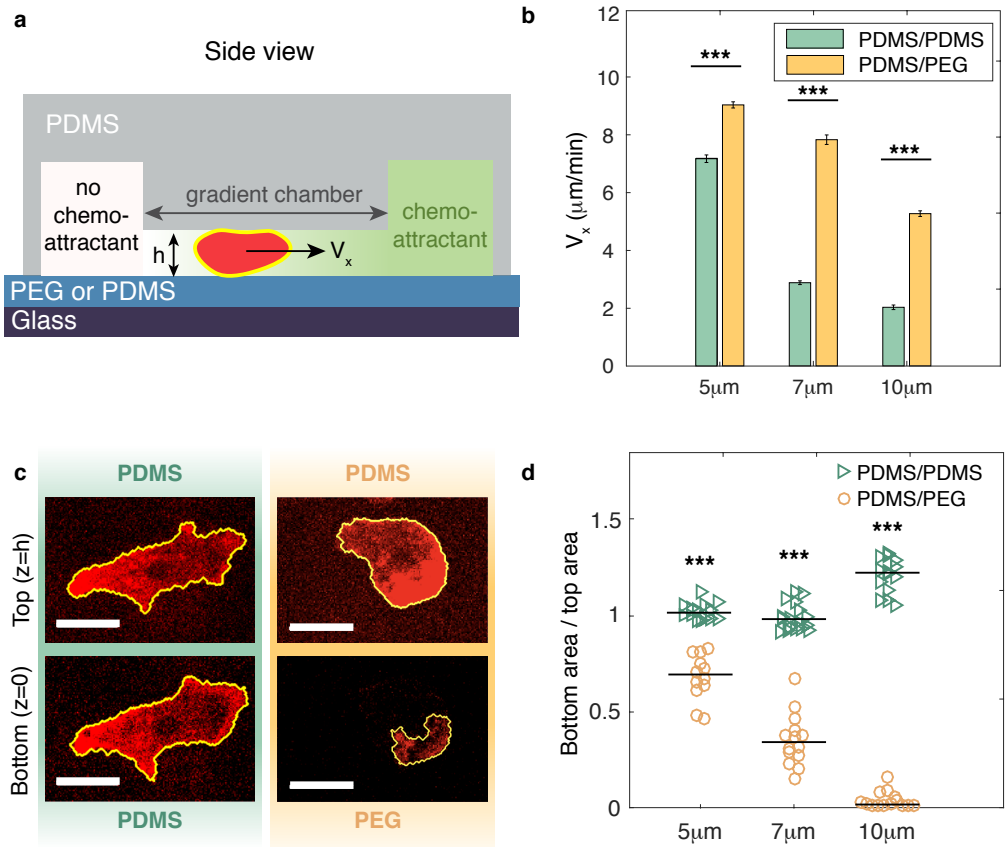

Fig. 5 Experimental tests of the numerical and theoretical predictions. **a**. Schematic side view of the microfluidics chamber. Cells are placed in a confined chamber with variable height. The top substrate is composed of PDMS while the bottom substrate is either composed of PDMS or coated with less adhesive PEG. Cells are guided by a chemoattractant (cAMP) gradient of strength 0.45 nM/μm in the chamber. **b**. Cell speed in the gradient direction for varying chamber height, indicated along the x-axis, and top/bottom substrate composition, indicated by the label. For both PDMS/PDMS and PDMS/PEG substrate compositions, the cell speed decreases as chamber height is increased. Furthermore, for fixed chamber height, cells move faster when the bottom substrate is less adhesive (i.e., PDMS/PEG). P-value $< 10^{-5}$ with unpaired t-test. Error bars represent the standard error of the mean. **c**. Scan of the cell area profile at the top and bottom of the chamber using the fluorescent membrane marker Car1-RFP ($h = 5\mu$m). Cells with PEG-coated bottom substrates (PDMS/PEG) show asymmetric shapes whereas cells with PDMS bottom substrates (PDMS/PDMS) show symmetric shapes. Scale bar, 10μm. **d**. Ratio of top and bottom contact area under different conditions (label indicates bottom substrate composition). P-value $< 10^{-5}$ with Wilcoxon rank-sum test.

age speed of the cell V_x in the direction of the chemoattractant gradient, both as a function of the height of the chamber and for different substrate compositions (Fig. 5b). Furthermore, to quantify the effect of the adhesive properties of the substrates on migrating cells, we measure the contact area of the cell on both top and bottom substrates of the chamber using confocal microscopy (Fig. 5c and d). More adhesive substrates will result in more cell spreading and thus larger contact areas.

Our theoretical predictions for cells in confinement are that decreased height increases speed, and that cells in asymmetric adhesion are faster than cells in symmetric adhesion. Both of these qualitative predictions are observed in our experiments. First, our experiments show that cell speed is significantly affected by the height of the chamber (Fig. 5b). Cells in chambers of height $h = 10\mu$m move markedly slower than cells in chambers with $h = 7\mu$m which, in turn, have smaller speed than cells in chambers with $h = 5\mu$m. The trend of slower motion in deeper chambers holds for both PDMS and PEG coated bottom substrates. Furthermore, we have verified that these results do not depend on the steepness of the gradient (Fig. S11). These observations are fully consistent with our numerical and theoretical predictions (Fig. 3).

In addition, our experiments show that cells moving in a chamber with unequal top and bottom adhesion are markedly asymmetric (Fig. 5c), consistent with past results that showed that *Dictyostelium* cells only weakly adhere to PEG. Specifically, the contact area of cells on PEG coated substrates is significantly smaller than the contact area on PDMS substrates and the resulting asymmetry can be quantified by the ratio of bottom and top contact area. Cells with PDMS on top and bottom and for $h = 5\mu$m and $h = 7\mu$m have ratios close to 1 indicating that the shape is symmetric. In contrast, cells moving in chambers with these values of h that have a PEG bottom have ratios that are much smaller than 1, indicating a more asymmetric cell shape. For the largest value of h ($h = 10\mu$m) cell preferentially attach to the top PDMS substrate, resulting in negligible contact area at the bottom PEG substrate and ratios close to 0. For this chamber height, the ratio for PDMS substrates is larger than one since cells are loaded on the bottom substrate and cannot fully attach to the top substrate.

Importantly, quantifying the cell speed for the different chambers reveals that cells in the symmetric PDMS/PDMS condition move slower than cells in the asymmetric PDMS/PEG condition (Fig. 5b). Again, these experimental results are fully consistent with our theoretical and numerical predictions and show that cell shape, and more specifically its effective height, can significantly affect motility speed (Fig. 3).

3 Discussion and conclusion

In this study, we examined how cell shape can affect cell speed using simulations, analytics, and experiments. We should stress that our experiments can only be compared to the simulations on a qualitative level. Values for the model parameters are not precisely known, and our model cell is not fully three-dimensional. Nevertheless, separating the frictional and adhesive force in the model provides clear insights into the role of adhesion and cell shape in determining cell speed. This separation also makes it challenging to compare our results to previous studies that investigated the effects of cell-substrate interactions on cell speed. For example, a recent study using fish keratocyte cells[22] found that cell spreading increases with adhesion strength (measured by the concentration of adhesive molecules). These experiments also revealed a biphasic speed dependence on adhesion such that cell speed increases between low and intermediate adhesion strengths and decreases between intermediate and high adhesion strengths. These results are similar to earlier experimental studies, and have previously been interpreted in terms of minimal models without cell shape[38,43,44]. Our results suggest that the increase of cell speed with increased adhesion found in these experiments might be attributed to cell spreading and a lower effective height. The observed decrease in cell speed following a further increase in adhesion can then be explained by a larger relative role of frictional forces. Likewise, our experimental results suggest that our experiments operate in a regime where substrate friction is less important than the internal viscosity and hence the major effect of the substrate modification is the change in adhesion.

Our numerical and experimental results indicate that changing cell morphology through confinement can also significantly alter the migration speed, with decreasing chamber heights resulting in increased cell speeds. Comparison with other cell types is challenging as cells might change their behavior following confinement. A recent study using normal human dermal fibroblast cells, for example, found that slow mesenchymal cells can spontaneously switch to a fast amoeboid migration phenotype under confinement[44]. This phenotypic transition makes it difficult to directly compare those observations with our results and further investigation is needed to determine how different cell types behave in confinement.

We should point out that the simple scaling of cell speed dependence on cell height (Eq. 6) is based on the assumption of localized active stress (the numerator) and uniform cytoskeleton viscosity (the denominator) in the entire cross section. As shown in our experimental work and in previous studies[32], F-actin is localized close to the substrate, in support of the first assumption. It is currently unclear whether the second approximation is valid for *Dictyostelium* or other cells. Presumably, in cells with a clear segregation of actin cortex and cytoplasm, a large viscosity contrast could be present. Nevertheless, our arguments might still hold, as long as passive regions are coupled to the active regions through shear interactions (one example is the model in Ref.[31]). In this case, passive regions will still slow down the cell, but the relation between cell speed and shape will be more complicated and will have contributions from regions with different viscosity. To address this more general case, a full three-dimension model with viscosity contrast between the cortex and cytoplasm is necessary and will be part of future extensions.

In summary, we show how adhesion forces result in cell spreading and that the accompanying shape changes can result in larger velocities. Key in this result is the existence of a narrow band of active stress that has a smaller spatial extent than the height of the cell. As a result, the dissipation due to the shear stress between this active band and the remainder of the cell increases as the effective height of the cell increases. In our model, we

have assumed a cell motility model corresponding to stable flat protrusions. The conclusion that cell speed scales inversely with the effective height is also valid for other cell motility models as long as the active propulsion region has limited spatial extent. For example, replacing the constant active stress by an oscillating stress, similar to protrusion-retraction cycles seen in amoeboid cells, does not change the qualitative results (Fig. S12). Further extensions of our model could include focal adhesive complexes (to model a broader range of eukaryotic cell types) and different types of actin structures in different parts of the cell. These extensions can then be used to further determine the role of adhesion in cell motility.

References

1 A. Munjal and T. Lecuit, *Development*, 2014, **141**, 1789–1793.
2 V. Kölsch, P. G. Charest and R. A. Firtel, *J Cell Sci*, 2008, **121**, 551–559.
3 D. Wirtz, K. Konstantopoulos and P. C. Searson, *Nature Reviews Cancer*, 2011, **11**, 512–522.
4 B. Geiger, J. P. Spatz and A. D. Bershadsky, *Nature reviews Molecular cell biology*, 2009, **10**, 21–33.
5 G. Charras and E. Sahai, *Nature reviews Molecular cell biology*, 2014, **15**, 813.
6 C. E. Chan and D. J. Odde, *Science*, 2008, **322**, 1687–1691.
7 A. K. Harris, P. Wild and D. Stopak, *Science*, 1980, **208**, 177–179.
8 T. Frisch and O. Thoumine, *Journal of biomechanics*, 2002, **35**, 1137–1141.
9 K. Keren, Z. Pincus, G. M. Allen, E. L. Barnhart, G. Marriott, A. Mogilner and J. A. Theriot, *Nature*, 2008, **453**, 475–480.
10 C. A. Reinhart-King, M. Dembo and D. A. Hammer, *Biophysical journal*, 2005, **89**, 676–689.
11 J. Kockelkoren, H. Levine and W.-J. Rappel, *Physical Review E*, 2003, **68**, 037702.
12 F. Ziebert and I. S. Aranson, *PloS one*, 2013, **8**, e64511.
13 E. Tjhung, A. Tiribocchi, D. Marenduzzo and M. Cates, *Nature communications*, 2015, **6**, 5420.
14 Y. Zhao, S. Das and Q. Du, *Physical Review E*, 2010, **81**, 041919.
15 W. Mickel, L. Joly and T. Biben, *The Journal of chemical physics*, 2011, **134**, 094105.
16 A. Carlsson, *New journal of physics*, 2011, **13**, 073009.
17 A. Stéphanou, E. Mylona, M. Chaplain and P. Tracqui, *Journal of theoretical biology*, 2008, **253**, 701–716.
18 A. Mogilner, *Journal of mathematical biology*, 2009, **58**, 105.
19 M. Buenemann, H. Levine, W. J. Rappel and L. M. Sander, *Biophys J*, 2010, **99**, 50–58.
20 S. Alonso, M. Stange and C. Beta, *PloS one*, 2018, **13**, e0201977.
21 B. Rubinstein, M. F. Fournier, K. Jacobson, A. B. Verkhovsky and A. Mogilner, *Biophysical journal*, 2009, **97**, 1853–1863.
22 E. L. Barnhart, K.-C. Lee, K. Keren, A. Mogilner and J. A. Theriot, *PLoS biology*, 2011, **9**, e1001059.
23 J. S. Bois, F. Jülicher and S. W. Grill, *Physical review letters*, 2011, **106**, 028103.
24 D. Shao, H. Levine and W.-J. Rappel, *Proc Natl Acad Sci U S A*, 2012, **109**, 6851–6856.
25 B. A. Camley, Y. Zhao, B. Li, H. Levine and W.-J. Rappel, *Physical Review Letters*, 2013, **111**, 158102.
26 T. L. Goff, B. Liebchen and D. Marenduzzo, *arXiv preprint arXiv:1712.03138*, 2017.
27 D. Shao, W.-J. Rappel and H. Levine, *Physical Review Letters*, 2010, **105**, 108104.
28 S. Najem and M. Grant, *Physical Review E*, 2013, **88**, 034702.
29 T. Biben, K. Kassner and C. Misbah, *Physical Review E*, 2005, **72**, 041921.
30 K. A. Brakke, *Experimental mathematics*, 1992, **1**, 141–165.
31 K. Kruse, J. Joanny, F. Jülicher and J. Prost, *Physical biology*, 2006, **3**, 130.
32 O. Nagel, C. Guven, M. Theves, M. Driscoll, W. Losert and C. Beta, *PloS one*, 2014, **9**, e113382.
33 H. Tanimoto and M. Sano, *Biophysical journal*, 2014, **106**, 16–25.
34 A. R. Bausch, F. Ziemann, A. A. Boulbitch, K. Jacobson and E. Sackmann, *Biophys. J.*, 1998, **75**, 2038–2049.
35 M. Srinivasan and S. Walcott, *Physical Review E*, 2009, **80**, 046124.
36 S. Walcott and S. X. Sun, *Proc Natl Acad Sci U S A*, 2010, **107**, 7757–7762.
37 A. Huttenlocher, M. H. Ginsberg and A. F. Horwitz, *The Journal of cell biology*, 1996, **134**, 1551–1562.
38 S. P. Palecek, J. C. Loftus, M. H. Ginsberg, D. A. Lauffenburger, A. F. Horwitz *et al.*, *Nature*, 1997, **385**, 537–540.
39 M. L. Gardel, B. Sabass, L. Ji, G. Danuser, U. S. Schwarz and C. M. Waterman, *J cell Biol*, 2008, **183**, 999–1005.
40 W. F. Loomis, D. Fuller, E. Gutierrez, A. Groisman and W.-J. Rappel, *PloS one*, 2012, **7**, e42033.
41 M. Skoge, H. Yue, M. Erickstad, A. Bae, H. Levine, A. Groisman, W. F. Loomis and W.-J. Rappel, *Proc Natl Acad Sci U S A*, 2014, **111**, 14448–53.
42 T. Tzvetkova-Chevolleau, E. Yoxall, D. Fuard, F. Bruckert, P. Schiavone and M. Weidenhaupt, *Microelectronic Engineering*, 2009, **86**, 1485–1487.
43 P. A. DiMilla, K. Barbee and D. A. Lauffenburger, *Biophys. J.*, 1991, **60**, 15 – 37.
44 Y.-J. Liu, M. Le Berre, F. Lautenschlaeger, P. Maiuri, A. Callan-Jones, M. Heuzé, T. Takaki, R. Voituriez and M. Piel, *Cell*, 2015, **160**, 659–672.